

Neutron Scattering and Spectroscopic Studies of Hydrogen Adsorption in $\text{Cr}_3(\text{BTC})_2$ —A Metal–Organic Framework with Exposed Cr^{2+} Sites

Kenji Sumida,[†] Jae-Hyuk Her,^{‡,§,⊥} Mircea Dinca,^{†,¶} Leslie J. Murray,^{†,○} Jennifer M. Schloss,^{||} Christopher J. Pierce,^{||} Benjamin A. Thompson,^{||} Stephen A. FitzGerald,^{*||} Craig M. Brown,^{*§} and Jeffrey R. Long^{*†}

[†]Department of Chemistry, University of California, Berkeley, California 94720, and Materials Sciences Division, Lawrence Berkeley National Laboratory, Berkeley, California 94720

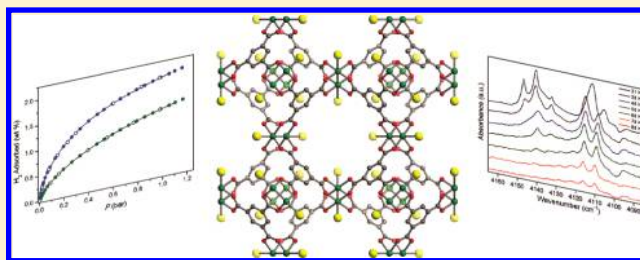
[‡]Department of Materials Science and Engineering, University of Maryland, College Park, Maryland 20742

[§]National Institute of Standards and Technology, Center for Neutron Research, Gaithersburg, Maryland 20899

^{||}Department of Physics, Oberlin College, Oberlin, Ohio 44074

Supporting Information

ABSTRACT: Microporous metal–organic frameworks possessing exposed metal cation sites on the pore surface are of particular interest for high-density H_2 storage at ambient temperatures, owing to the potential for H_2 binding at the appropriate isosteric heat of adsorption for reversible storage at room temperature (ca. -20 kJ/mol). The structure of $\text{Cr}_3(\text{BTC})_2$ ($\text{BTC}^{3-} = 1,3,5\text{-benzenetricarboxylate}$) consists of dinuclear paddlewheel secondary building units connected by triangular BTC^{3-} bridging ligands to form a three-dimensional, cubic framework. The fully desolvated form of the compound exhibits BET and Langmuir surface areas of 1810 and 2040 m^2/g , respectively, with open axial Cr^{2+} coordination sites on the paddlewheel units. Its relatively high surface area facilitates H_2 uptakes (1 bar) of 1.9 wt % at 77 K and 1.3 wt % at 87 K, and a virial-type fitting to the data yields a zero-coverage isosteric heat of adsorption of $-7.4(1)$ kJ/mol. The detailed hydrogen loading characteristics of $\text{Cr}_3(\text{BTC})_2$ have been probed using both neutron powder diffraction and inelastic neutron scattering experiments, revealing that the Cr^{2+} site is only partially populated until a marked elongation of the Cr–Cr internuclear distance occurs at a loading of greater than 1.0 D_2 per Cr^{2+} site. Below this loading, the D_2 is adsorbed primarily at the apertures of the octahedral cages. The H–H stretching frequency corresponding to H_2 molecules bound to the primary site is observed in the form of an *ortho*–*para* pair at 4110 and 4116 cm^{-1} , respectively, which is significantly shifted compared to the frequencies for free H_2 of 4155 and 4161 cm^{-1} . The infrared data have been used to compute a site-specific binding enthalpy for H_2 of $-6.7(5)$ kJ/mol, which is in agreement with the zero-coverage isosteric heat of adsorption derived from gas sorption isotherm data.



INTRODUCTION

Metal–organic frameworks have attracted significant interest in recent years, in part owing to their potential applications in gas storage, molecular separations, and heterogeneous catalysis.¹ In particular, the ability to construct these materials from the combination of a judiciously selected metal ion and organic bridging unit may provide a versatile platform for the preparation of materials possessing physical and chemical properties that are finely tuned for specific applications. With regard to hydrogen storage for mobile applications, gravimetric and volumetric storage densities approaching those prescribed by the U.S. Department of Energy² have been observed within the highest surface-area metal–organic frameworks at cryogenic temperatures.³ However, the storage capacity within these materials greatly diminishes at ambient temperature owing to the weak physisorptive interactions that predominate between H_2 and the framework surface. Indeed, the zero-coverage isosteric heat

of adsorption within these materials typically lies in the range of -5 to -7 kJ/mol, which is far below the -15 kJ/mol considered optimal over the entire adsorption range for an adsorbent operating between 1.5 and 30 bar at 298 K.⁴ Furthermore, the inclusion of an enthalpy–entropy correlation increases this magnitude even further, suggesting an optimal enthalpy of adsorption in the range of -20 to -25 kJ/mol.⁵

One strategy for improving the isosteric heat of H_2 adsorption within metal–organic frameworks is the synthesis of materials possessing open metal cation sites on the pore surface.⁶ Here, the charge of the cation serves to induce a dipole on the H_2 molecule, resulting in an electrostatic interaction that is stronger than the

Received: January 21, 2011

Revised: March 7, 2011

Published: March 25, 2011

dispersion-type interactions that predominate for physisorbed molecules.^{6,7} Indeed, a zero-coverage isosteric heat of H₂ adsorption as high as −15.1 kJ/mol has been demonstrated within the material Co₄(H₂O)₄(MTB)₂ (H₄MTB = methanetetra benzoic acid), which features unsaturated Co²⁺ sites following activation.⁸ However, in this case, the isosteric heat rapidly decreases as a function of surface coverage, indicating that the density of strong binding sites is a crucial factor in facilitating large H₂ storage capacities at 298 K.⁹ Thus, increasing the density of open metal sites remains a significant synthetic challenge, and a substantial body of recent computational work has been devoted to identifying potential candidate materials.¹⁰

The microporous metal–organic framework Cr₃(BTC)₂ (Figure 1, H₃BTC = 1,3,5-benzenetricarboxylic acid)¹¹ features a cubic network (space group: *Fm-3m*) of dinuclear paddlewheel units linked by triangular BTC^{3−} organic bridging units to form a (3,4)-net that is isostructural with M₃(BTC)₂ (M = Cu, Mo).^{12,13} Here, six paddlewheel units and four BTC^{3−} ligands form octahedral cages that share vertices to form a three-dimensional pore system resembling the boracite net topology. Upon desolvation of the solid by heating *in vacuo*, the material possesses unsaturated Cr²⁺ sites at the paddlewheel units. The presence of these sites has recently been demonstrated to afford tremendous adsorption selectivity for O₂ over N₂, owing to the ability of the metal centers to engage in a partial electron transfer with O₂, but not N₂.¹¹ Although such an interaction was not expected to occur with H₂, the high charge density at these coordination sites could still be of benefit for H₂ adsorption. Herein, we report the H₂ storage properties of Cr₃(BTC)₂, as probed through low-pressure adsorption experiments, infrared spectroscopy, and neutron scattering studies. The complementary nature of the experiments offers a greater depth in the description of H₂ adsorption within the material, and results in a more complete understanding of the influence of various chemical and structural features on the adsorption properties.

EXPERIMENTAL SECTION

General Considerations.¹⁴ Cr₃(BTC)₂ was synthesized and activated according to the literature procedure.¹¹ All reagents were obtained from commercial vendors, and used without further purification. All powder X-ray diffraction patterns were collected using a Bruker D8 Advance diffractometer (Cu K_α; λ = 1.5406 Å) equipped with a capillary stage. Owing to the air and moisture sensitivity of Cr₃(BTC)₂, all manipulations were performed within a glovebox under a dinitrogen or argon atmosphere. Note that even brief exposure of the compound to the air induces an immediate color change of the solid to a dark forest green color, which is accompanied by a loss of crystallinity and porosity. The isosteric heat of H₂ adsorption was calculated using the method reported previously.^{6f}

Low-Pressure Gas Sorption Measurements. Glass sample tubes of a known weight were loaded with approximately 100 mg of sample, and sealed using a TranSeal. Samples were degassed at 160 °C for 24 h on a Micromeritics ASAP 2020 analyzer until the outgas rate was no more than 1 mTorr/min. The degassed sample and sample tube were weighed precisely and then transferred back to the analyzer. The outgas rate was again confirmed to be less than 1 mTorr/min. H₂ adsorption isotherms were measured at 77 K in a liquid nitrogen bath and at 87 K in a liquid argon bath.

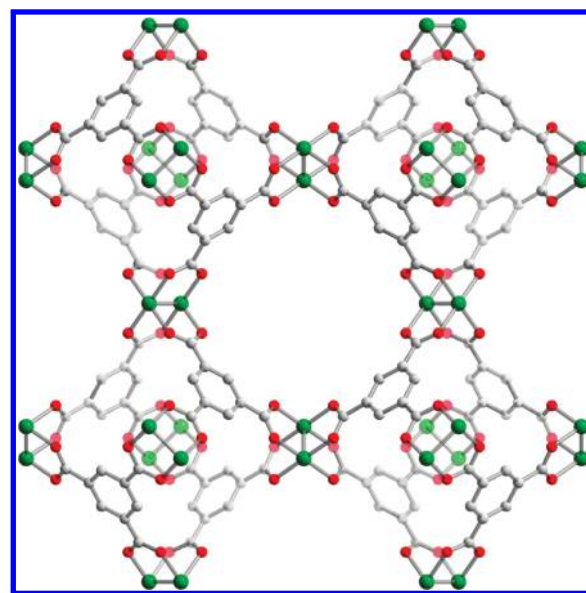


Figure 1. A portion of the crystal structure of evacuated Cr₃(BTC)₂. Green, gray, and red spheres represent Cr, C, and O atoms, respectively. Hydrogen atoms have been omitted for clarity.

Neutron Powder Diffraction Measurements. Neutron powder diffraction data were collected on the high resolution neutron powder diffractometer BT-1 at the National Institute of Standards and Technology (NIST) Center for Neutron Research (NCNR) with a Ge-(311) monochromator and using in-pile collimation of 15 min of arc, corresponding to a wavelength of 2.0782 Å. Measurements were taken as a function of deuterium loading (0.5, 1.0, 1.5, 2.0, and 3.0 D₂ molecules per Cr²⁺ site, loading performed at ca. 60 K) at a temperature of ca. 4 K with a measurement time of ca. 9 h. Note that D₂ is used rather than H₂ owing to the large incoherent scattering cross section of H₂, which results in an increased background and poorer quality diffraction data. The minor differences in properties between H₂ and D₂, most notably their zero-point energies, are not expected to significantly affect the adsorption behavior within the framework in the context of the diffraction studies.

All sample transfers were performed in a helium-filled glovebox equipped with water and oxygen monitors. Initial sample activation was performed in a glass tube with a packless bellows valve attached. The sample was evacuated using a turbomolecular pump (10^{−5} Torr) and heated to 150 °C for 48 h, after which time the sample was cooled and transferred to a cylindrical vanadium can equipped with a capillary gas line and a packless valve, and sealed with an indium O-ring. The sample was mounted onto a sample stick equipped with a stainless-steel gas line with an additional valve for a top-loading closed-cycle helium refrigerator. The sample was further degassed *in situ* under high vacuum to remove residual helium. During the experiments, a known amount of hydrogen (deuterium) gas was loaded into the sample (1.174 g), which was typically maintained at a temperature of 60 K (CCR) until no pressure drop was observed for at least 1 min. The sample was then cooled down to the base temperature of 3.5 K over a period of 1 h in order to perform measurements. In all cases, the outgas pressure reading was zero well before reaching 25 K.

Neutron powder diffraction patterns were analyzed using the Rietveld refinement method. The program EXPGUI¹⁵ incorporating

the Rietveld program GSAS¹⁶ was used to perform all refinements. The model of the bare material was refined first, and was used as the starting point for subsequent refinements of the D₂-loaded samples. In all cases, D₂ molecules were treated as point scatterers with double occupancy in accord with the rotationally disordered quantum mechanical molecule.¹⁷ The coordinates of all other atoms and the displacement parameters were allowed to vary during the refinement of each D₂ loading case. On the basis of the structure obtained from the diffraction pattern of the bare material, the diffraction patterns of the first D₂-loaded case (0.5 D₂ molecules per Cr²⁺) were analyzed by first neglecting the D₂ molecules. The Fourier difference maps were calculated, clearly indicating the positions of D₂ adsorption sites. Accurate values for the D₂ locations and occupancy numbers were then obtained by Rietveld refinement after incorporating the D₂ molecules into the structure model. For each successive D₂ loading, the Fourier difference map was calculated on the basis of the results of the previous D₂ loading and used to identify new D₂ adsorption sites.

Inelastic Neutron Scattering (INS) Spectroscopy. The INS spectra were measured at 4 K using the pyrolytic graphite monochromator and 20'–20' collimation options on the BT-4 filter analyzer neutron spectrometer (FANS)¹⁸ at the NCNR. The sample (1.174 g) was sealed in a cylindrical aluminum cell suitable for *in situ* gas loading and cooled in a CCR. H₂ gas was used during the measurements to take advantage of its large incoherent neutron scattering cross section. Note that the H₂ molecule is a very good quantum rotor due to its light mass and consists of two indistinguishable fermions (protons) that require the wave function to be antisymmetric. If the nuclear spins of two protons are antiparallel, H₂ is said to be in a *para* state (*p*-H₂); otherwise, it is in an *ortho* state (*o*-H₂). The quantum rotation number, *J*, of a H₂ molecule thus has to be even for a *para*-H₂ and odd for an *ortho*-H₂. At room temperature, only one-fourth of H₂ molecules are in the *para* state. Usually, the conversion rate between states is very slow but can be greatly accelerated in the presence of a fluctuating magnetic moment. Both *p*-H₂ and normal H₂ (*n*-H₂), which consists of 25% *p*-H₂ and 75% *o*-H₂, were used in these experiments.

A neutron scattered by a H₂ molecule can induce the required nuclear spin flip to convert a *para/ortho* H₂ to an *ortho/para* H₂. This *para*–*ortho* or *ortho*–*para* transition is associated with the change of the rotational quantum number, *J*, from even/odd to odd/even, and has a large neutron scattering cross section that is proportional to the incoherent neutron scattering cross section of the proton. INS spectra of the adsorbed H₂ were obtained by subtracting the INS spectrum of the bare materials. For a free hydrogen molecule, the *para*–*ortho* transition is usually associated with the *J* = 0 to *J* = 1 excitation occurring with an energy of 14.7 meV, which can be directly measured by INS but not optical spectroscopies. The local potential of a host material will generate rotational barriers for the adsorbed H₂ which typically cause the *J* = 1 state to split into its three sublevels. Additionally, the translation excitations of the H₂ molecule may be coupled to the rotational transition and complicate the observed spectra. Hence, the INS spectra of adsorbed H₂ may show complex features with multiple peaks in the spectrum containing rich information about the host material and the hydrogen interactions.

Loadings of 0.5, 1.0, 2.0, and 3.0 *p*-H₂ and *n*-H₂ per Cr²⁺ site were performed at 70 K with data collection at 4 K. Data were collected for approximately 9 h per loading. The energy resolution is between 1.2 and 2.0 meV over the energy transfer ranges accessible. Data reduction, including the subtraction of the bare

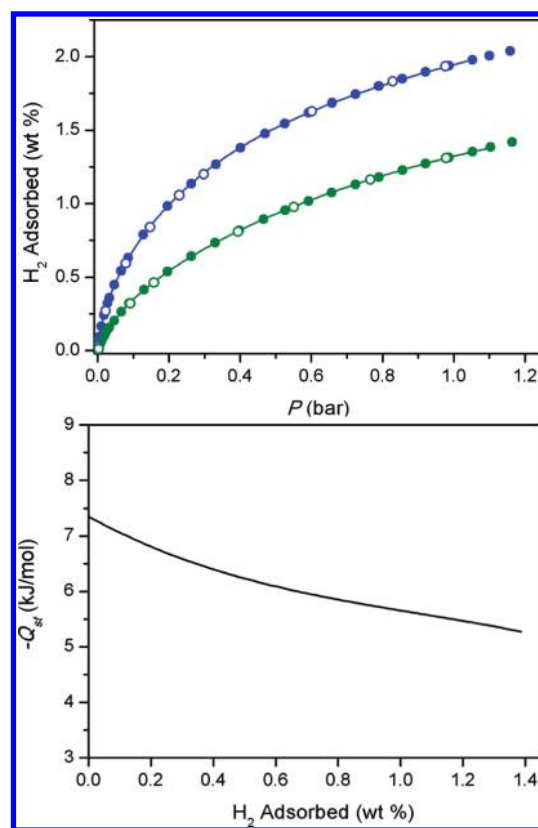


Figure 2. (upper) Lower-pressure H₂ isotherms in Cr₃(BTC)₂ collected at 77 K (blue) and 87 K (green). Closed and open symbols represent adsorption and desorption, respectively, and the solid lines represent a virial-type fitting to the data. (lower) A plot of the isosteric heat of adsorption as a function of H₂ coverage.

Cr₃(BTC)₂ spectrum from the H₂-loaded spectra, and peak fitting, were performed within the DAVE software suite.¹⁹

Infrared Spectroscopy. Infrared spectra were acquired using a Bomem DA3 Michelson interferometer equipped with a quartz-halogen source, a CaF₂ beamsplitter, and a liquid nitrogen cooled mercury-cadmium-telluride detector. A custom-built diffuse reflectance system²⁰ with a sample chamber that allows both the temperature and atmosphere of the material to be controlled was utilized for all experiments. Powder samples of Cr₃(BTC)₂ (ca. 10 mg) were transferred under an inert atmosphere to a cup affixed to a copper slab providing thermal contact to a coldfinger cryostat (Janis ST-300T). The sample temperature was monitored by a Si-diode thermometer placed directly within the sample cup. Prior to introduction of the hydrogen gas, the samples were evacuated for several hours at room temperature. Known quantities of research grade (99.9999% purity) H₂ were dispensed from a calibrated gas manifold by monitoring the change in pressure.

RESULTS AND DISCUSSION

H₂ Adsorption Isotherms. The H₂ adsorption isotherms collected for an activated sample of Cr₃(BTC)₂ are presented in Figure 2. The relatively high BET surface area of 1810 m²/g facilitates a reversible adsorption (1 bar) of 1.9 and 1.3 wt % at 77 and 87 K, respectively. The zero-coverage isosteric heat of adsorption (*Q*_{st}) for H₂ obtained from a virial-type fitting to the isotherm data of −7.4(2) kJ/mol represents just a slight increase in

the magnitude of Q_{st} compared to materials that do not feature exposed cation sites. As discussed below, the neutron powder diffraction data reveal that the Cr^{2+} sites are occupied only at high loadings following a slight elongation of the Cr–Cr distance within the paddlewheel unit. As a result, this leads to the occupation of a single binding site that facilitates short contacts with the organic component of the framework at low coverage, which is consistent with the relatively small magnitude of Q_{st} . Note that this serves to highlight one of the primary disadvantages of the analysis of bulk isotherm data, as is often performed in adsorption studies, since conclusions regarding the binding environment of H_2 within the framework cannot be deduced directly, particularly in cases where the site-specific adsorption enthalpies of two or more sites within the unit cell are quite similar. Nevertheless, the value of Q_{st} at zero coverage is comparable to the corresponding value reported for $\text{Cu}_3(\text{BTC})_2$ (-6.8 kJ/mol).²¹ Consistent with the successive occupancy of the strongest binding sites within

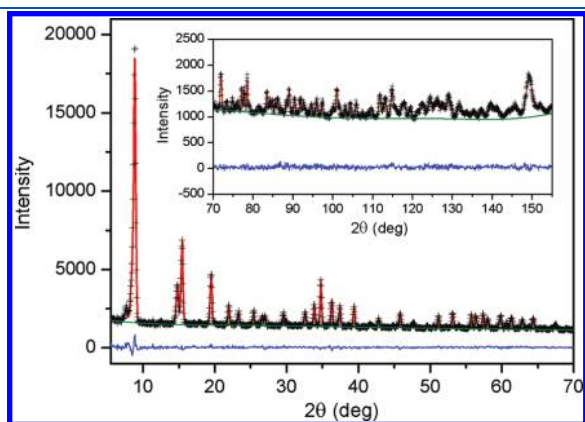


Figure 3. Representative neutron powder diffraction data, collected for $\text{Cr}_3(\text{BTC})_2$ following a dosing of 0.5 D_2 molecules per Cr^{2+} site. Green lines, crosses, and red lines represent the background, experimental, and calculated diffraction patterns, respectively. The blue line represents the difference between experimental and calculated patterns. The final Rietveld goodness-of-fit parameter was $\chi^2 = 0.9329$.

$\text{Cr}_3(\text{BTC})_2$, the magnitude of Q_{st} gradually decreases to $-5.7(2)$ kJ/mol at a H_2 uptake of 1.0 wt %. A complete analysis of the coverage-dependent adsorption characteristics and binding sites within the material is explored in detail below in the context of neutron powder diffraction, inelastic neutron scattering spectroscopy, and infrared spectroscopy.

Neutron Powder Diffraction Data. Rietveld analysis of the bare $\text{Cr}_3(\text{BTC})_2$ material revealed the expected cubic network of dinuclear paddlewheel secondary building units bridged by 3-connected organic linkers (Figure 1). Significantly, the short Cr–Cr distance of 2.06(2) Å is indicative of the presence of a metal–metal quadruple bond, and results in the Cr^{2+} being situated approximately 0.11(2) Å below the four-atom mean plane formed by the oxygen atoms of the carboxylate ligands. We note that, in the fully evacuated state, no nuclear density was observed on the axial coordination sites on the Cr^{2+} centers, reflecting the removal of all of the coordinated solvent molecules, and full activation of the pores.

The D_2 binding sites within $\text{Cr}_3(\text{BTC})_2$ were determined by successively dosing the evacuated material with D_2 at loadings corresponding to 0.5, 1.0, 1.5, 2.0, and 3.0 D_2 molecules per Cr^{2+} center, and taking nuclear density Fourier difference maps between the loaded and evacuated materials. Any new locations were added to the Rietveld process where the final positions and occupancies of the D_2 molecules were allowed to refine freely. Note that, at each loading level, the total refined occupancy of D_2 assigned from the neutron density map agrees well with the expected total occupancy, indicating full assignment of all of the binding sites within the unit cell (Tables S2–S6, Supporting Information).

The neutron diffraction data and Rietveld refinement results for data collected at a loading of 0.5 D_2 molecules per Cr^{2+} site are shown in Figure 3. Surprisingly, no nuclear density was observed at the open Cr^{2+} site at this loading level, and the D_2 is located in the apertures of the octahedral cages at a distance of approximately 4 Å from the carbon atoms of the aryl rings of the BTC^{3-} ligands (Figure 4B, site I). Upon increasing the loading to 1.0 D_2 molecules per Cr^{2+} site, additional nuclear density was observed at site I, as well as a small quantity at the open Cr^{2+} site

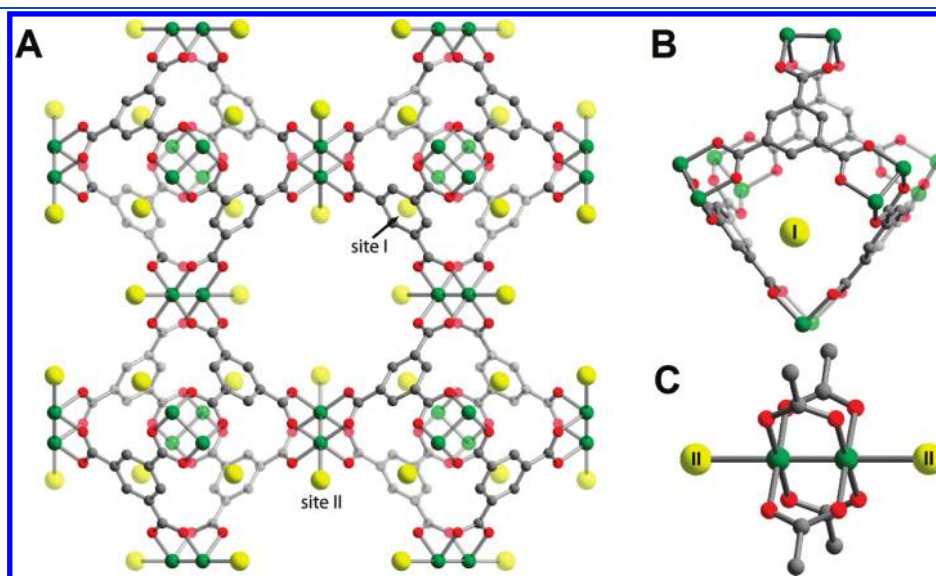


Figure 4. A portion of the structure of $\text{Cr}_3(\text{BTC})_2$ showing the first two D_2 binding sites, where green, red, and gray spheres represent Cr, O, and C atoms, respectively, while large yellow spheres represent D_2 molecules (A). The first occupied position (site I) is located at the apertures of the octahedral cages (B), while, at higher loadings, the unsaturated Cr^{2+} center (site II) is occupied (C).

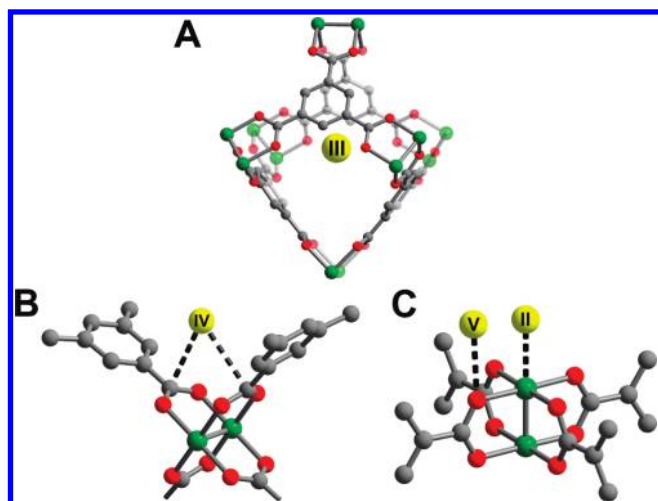


Figure 5. D₂ binding sites III–V observed within Cr₃(BTC)₂ at higher loadings. Site III (A) lies in the center of the octahedral cages, site IV (B) resides within a V-shaped binding pocket between two BTC^{3−} moieties, while site V (C) is situated in close contact (ca. 2.7 Å) with the oxygen atom of the carboxylate group.

(Figure 4C, site II). Here, the D₂ is disposed at a distance of 2.63(2) Å from the Cr²⁺ center, which is significantly greater than the corresponding distance of 2.39(1) Å observed in Cu₃(BTC)₂,²² and is also longer than those observed for other frameworks featuring exposed metal cation sites.²³ This is consistent with the larger ionic radius of Cr²⁺ (0.80 Å; high spin) compared to Cu²⁺ (0.73 Å), yielding a lower charge density and subsequently a weaker induced dipole on the adsorbed D₂ molecules.²⁴ Furthermore, the Cu–Cu distance in Cu₃(BTC)₂ is significantly longer than the Cr–Cr distance in Cr₃(BTC)₂, which results in the Cu²⁺ ions projecting out into the pores of the framework. This likely allows the D₂ molecules to interact more directly with the metal centers due to the lower steric demand of these sites. Here, the apparent preference for D₂ to populate site I rather than site II at the lowest loadings is probably a result of a combination of the Cr²⁺ binding site being sterically less accessible to guest molecules and the binding energy at the open metal site being comparable to that of site I. Nevertheless, to our knowledge, Cr₃(BTC)₂ is the first example of a metal–organic framework furnished with open metal sites wherein the metal center is not the favored binding site for D₂ at low coverages.

Interestingly, upon increasing the D₂ loading from 1.0 to 1.5 D₂ molecules per Cr²⁺ center, an elongation of the Cr–Cr distance from 2.06(2) to 2.17(2) Å is observed, representing a decrease in the bond order of the Cr–Cr interaction. This serves to project the Cr²⁺ cations above the four-atom mean plane of the oxygen atoms of the carboxylate moieties. Importantly, this structural change is accompanied by a reorganization of the nuclear density after the next dosing step such that site II is fully populated, suggesting that the D₂ molecules are able to more readily access the open metal site once it is projected out into the channels. Note that the sample is warmed to approximately 60 K during each dosing step, allowing the D₂ molecules to migrate more rapidly to their preferred positions following the structural change. Furthermore, at this loading level, additional nuclear density is also observed at the center of the octahedral cages (Figure 5A, site III), and is observed at full occupancy. As the

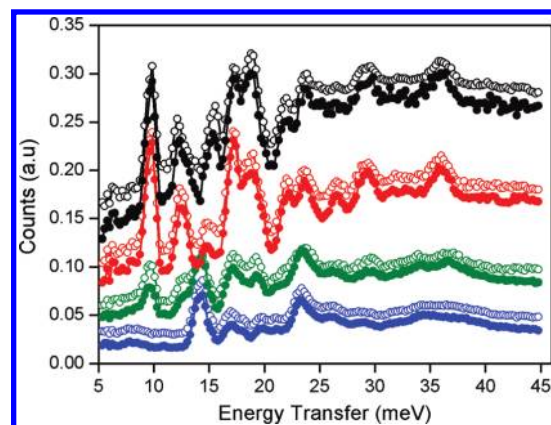


Figure 6. Selected inelastic neutron scattering (INS) spectra recorded at 4 K following subtraction of the spectrum of evacuated Cr₃(BTC)₂ for loadings of 0.5 (blue), 1.0 (green), 2.0 (red), and 3.0 (black) H₂ molecules per Cr²⁺ site. Filled and open symbols represent data for *p*-H₂ and *n*-H₂, respectively.

loading is increased further to 2.0 and 3.0 D₂ molecules per Cr²⁺ site, additional nuclear density appears, corresponding to close contacts in the channels of the framework. As shown in Figure 5B, site IV is positioned in a V-shaped binding pocket formed by two carboxylate moieties of the paddlewheel units, wherein the D₂ molecule is disposed approximately 3.3 Å from the framework surface. Meanwhile, site V (Figure 5C) is observed approximately 2.8 Å from the oxygen atoms of the carboxylate moieties, although only a small occupancy is observed at this site even at the highest loadings. Previous studies performed on Cu₃(BTC)₂ revealed adsorption sites with coordinates and interaction distances similar to sites III–V observed here,²² which might be anticipated on the basis of the isostructural nature of the two frameworks.

Inelastic Neutron Scattering Spectra. The H₂ loading characteristics of Cr₃(BTC)₂ were examined in further detail by inelastic neutron scattering. Data were collected at the same loadings (0.5, 1.0, 2.0, and 3.0 H₂ molecules per Cr²⁺ site) as for the neutron powder diffraction experiments to allow for the best opportunity for correlation of FANS spectra with the binding sites observed crystallographically. For all spectra, routine data reduction and subtraction of the spectrum for the evacuated form of Cr₃(BTC)₂ was performed, and selected spectra are displayed in Figure 6.

At the lowest loading of 0.5 H₂ per Cr²⁺ site, a sharp peak is observed at 14.3 meV. This feature is consistent with the first transition between rotational energy levels, $J = 0 \rightarrow 1$, of an almost unhindered H₂ molecule, and presumably corresponds to the molecules located in the windows of the octahedral cages (site I). The lack of a significant shift for these molecules from the corresponding signal for free H₂ observed at 14.7 meV is presumably due to the relatively large distance between H₂ and the framework surface, resulting in only a small increase in the rotational barrier of the H₂ molecule upon occupation of site I. A broader feature is also observed at 23.0 meV, which is likely due to the rotation of H₂ coupled with a phonon of approximately 9 meV as observed in Cu₃(BTC)₂.¹⁷ The overall similarity of the *n*-H₂ and *p*-H₂ spectra indicates that the normal hydrogen is converted from the $J = 1$ *ortho* form to the $J = 0$ *para* form, and this is mirrored for all loadings, even in the cases where the strongest accessible adsorption site is not the metal center. This

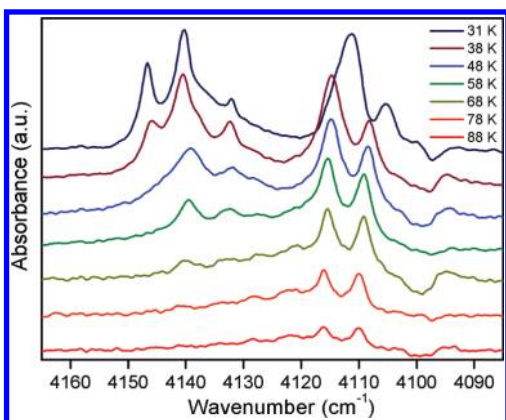


Figure 7. Selected variable-temperature infrared spectra (Q-region) for $\text{Cr}_3(\text{BTC})_2$ following dosing with H_2 collected at temperatures between 31 and 88 K at a resolution of 1 cm^{-1} . Spectra are offset for clarity.

suggests that virtually all of the H_2 molecules are able to approach the paramagnetic Cr^{2+} ion with a sufficient proximity for *ortho*–*para* conversion.

Upon increasing the loading to 1.0 H_2 per Cr^{2+} site, a sharp feature at 9.6 meV is observed. This peak is assigned to H_2 molecules bound to the unsaturated Cr^{2+} sites (site II), which experience a significant rotational hindrance due to the close approach of these molecules to the framework surface, as observed in the neutron powder diffraction experiments. Rotational transitions are also apparent at energies close to this value for *p*- H_2 in $\text{Cu}_3(\text{BTC})_2$ where the initial adsorption is at the metal center.¹⁷ The corresponding growth of a peak at around 19 meV is clearly observed and was previously ascribed to a coupled rotation and phonon in $\text{Cu}_3(\text{BTC})_2$, which is likely also the case here. The intensities of these peaks increase following subsequent loadings to 2.0 and 3.0 H_2 per Cr^{2+} site, which is consistent with the eventual full occupation of molecules at this binding site.

Infrared Spectra. The adsorption of H_2 within $\text{Cr}_3(\text{BTC})_2$ was further probed through the collection of variable-temperature infrared spectra. An activated sample of $\text{Cr}_3(\text{BTC})_2$ was exposed to a total dosing of 4 H_2 per Cr^{2+} center. As the sample temperature was decreased, the H_2 pressure dropped to a base value of 0.01 bar at 30 K, indicating that virtually all of the dosed gas had adsorbed onto the framework. The spectra collected at different temperatures during this procedure are presented in Figure 7. As the temperature is lowered from 88 K, the emergence of a single *ortho*–*para* pair corresponding to the H–H stretch for H_2 molecules bound to the framework surface is observed at 4110 and 4116 cm^{-1} , respectively. Here, the presence of only a single band at 88 K suggests the occupancy of a single crystallographic site within the unit cell, which, based on the neutron powder diffraction and INS experiments, is presumably the site located at the aperture of the octahedral cages (site I).²⁵

Upon cooling of the sample below 58 K, a second *ortho*–*para* pair is observed at 4132 and 4141 cm^{-1} , respectively. These bands are consistent with the occupation of a secondary binding site that is less polarizing toward H_2 and, based upon the neutron diffraction data, is ascribed to adsorption of H_2 at the open Cr^{2+} site (site II). Note that the reorganization of the neutron density following elongation of the Cr–Cr bond as observed in the neutron powder diffraction experiments suggests that the

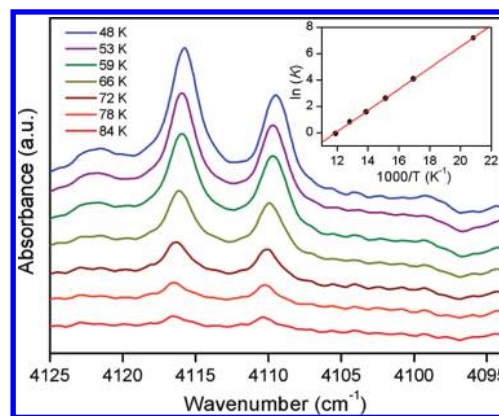


Figure 8. Selected variable-temperature infrared spectra of the *ortho*–*para* pair for H_2 adsorbed at the primary binding site within $\text{Cr}_3(\text{BTC})_2$ collected between 48 and 84 K at a resolution of 1 cm^{-1} . Spectra are offset for clarity. Inset: An Arrhenius law plot derived from the integrated absorbance from the spectral data.

interaction between H_2 and Cr^{2+} is not necessarily weaker than the adsorption enthalpy for H_2 at site I following the elongation of the Cr–Cr distance. This structural change, and the expected change in interaction energy, is expected to induce a shift in the position of the absorption band attributable to site II, owing to the change in the degree of activation of the H_2 molecules located at this site. However, the relatively constant position of the adsorption bands for H_2 at the Cr^{2+} site reveals that, under the conditions of the infrared experiments, such a structural change does not occur, possibly due to the significantly higher temperatures (and consequently small quantity of adsorbed H_2) under which the data were collected.

The evolution of a single peak at 4146 cm^{-1} is observed upon further cooling of the sample below 38 K. This new signal is attributed to adsorption of H_2 at the center of the octahedral cages (site III), which was observed at high loadings in the neutron powder diffraction experiments. Notably, the occupation of this site induces a shift in the infrared absorption band for H_2 located in the apertures of these cages (site I). This is presumably due to a change in the chemical environment for the H_2 molecules at site I, owing to the relatively short proximity (ca. 3.4 Å) of site III from this site.

The lowest-temperature infrared data obtained for an H_2 dosing of 1.1 H_2 per Cr^{2+} center are shown in Figure 8. The standard enthalpy of adsorption (ΔH^0) for the primary binding site was extracted by generating an Arrhenius-type plot from the integrated infrared absorbance as a function of temperature (see Figure 8, inset). The value of $-6.7(5) \text{ kJ/mol}$ is consistent with the relatively weak binding of H_2 at the primary binding site, and is significantly lower than the corresponding value obtained from a similar analysis for $\text{Cu}_3(\text{BTC})_2$ (-10.1 kJ/mol).^{12c} However, we note that the primary binding site in $\text{Cu}_3(\text{BTC})_2$ is at the open Cu^{2+} cation sites, which leads to a higher site-specific adsorption enthalpy. In addition, the standard enthalpy change ΔS^0 of $-78 \text{ J/mol}\cdot\text{K}$ is consistent with the close approach and efficient packing of the H_2 molecules on the framework surface. Note that the enthalpy–entropy correlation for H_2 adsorption is a significant factor in assessing the optimal value of ΔH^0 for metal–organic frameworks. The often-quoted optimal ΔH^0 value of ca. -15 kJ/mol is based on a constant $\Delta S^0 = 8R = -66.5 \text{ J/mol}\cdot\text{K}$,⁴ which is smaller in magnitude than the value

observed here, and values obtained via similar variable-temperature infrared spectroscopy studies of $\text{Cu}_3(\text{BTC})_2$, and other porous media. The consideration of the higher magnitude of ΔS^0 leads to the optimal value for ΔH^0 being in the range of -20 to -25 kJ/mol.⁵ Note that the value for ΔS^0 is binding-site-dependent, which suggests that the more a binding site imposes spatial ordering on the adsorbed H_2 molecule, a larger magnitude of ΔH^0 is required to overcome the entropy contribution. Thus, the preparation of a metal–organic framework for ambient H_2 storage applications requires careful consideration and fine-tuning of the thermodynamics of each binding site within the material.

Conclusions. The foregoing results demonstrate the hydrogen storage properties of $\text{Cr}_3(\text{BTC})_2$, a metal–organic framework possessing open Cr^{2+} sites, as probed through a combination of low-pressure adsorption, neutron powder diffraction, inelastic neutron scattering, and variable-temperature infrared experiments. Surprisingly, the loading characteristics differ significantly from those of the isostructural compound $\text{Cu}_3(\text{BTC})_2$, with full occupancy at the unsaturated Cr^{2+} center not being observed until a lengthening of the Cr–Cr distance also occurs at a loading of 1.5 D_2 per Cr^{2+} site. Although the low isosteric heat of adsorption in $\text{Cr}_3(\text{BTC})_2$ precludes its application as a room temperature hydrogen storage material, such a detailed understanding of the hydrogen sorption properties as probed through several complementary experimental techniques has revealed greater insight into the chemical and physical properties required for next-generation hydrogen storage materials.

■ ASSOCIATED CONTENT

Supporting Information. Full experimental details, neutron powder diffraction refinement data, infrared spectra (PDF), and crystallographic information files (CIF). This material is available free of charge via the Internet at <http://pubs.acs.org>.

■ AUTHOR INFORMATION

Present Addresses

[†]GE Global Research, Niskayuna, NY 12309.

[#]Department of Chemistry, Massachusetts Institute of Technology, Cambridge, Massachusetts, 02139.

[○]Department of Chemistry, University of Florida, Gainesville, Florida, 32611.

■ ACKNOWLEDGMENT

The research in Berkeley was funded by the Department of Energy under Contract No. DE-AC02-05CH11231. We acknowledge Fulbright New Zealand for partial support of K.S. The work at NIST was partially funded by the U.S. Department of Energy within the EERE Hydrogen Sorption Center of Excellence, and the work at Oberlin College was partially funded by the American Chemical Society Petroleum Research Fund. We thank Dr. Y. Liu for technical assistance during the neutron measurements.

■ REFERENCES

(1) (a) Eddaoudi, M.; Kim, J.; Rosi, N.; Vodak, D.; Wachter, J.; O’Keeffe, M.; Yaghi, O. M. *Science* **2002**, *295*, 469. (b) Matsuda, R.; Kitaura, R.;

Kitagawa, S.; Kubota, Y.; Belosludov, R. V.; Kobayashi, T. C.; Sakamoto, H.; Chiba, T.; Takata, M.; Kawazoe, Y.; Mita, Y. *Nature* **2005**, *436*, 238. (c) Millward, A. R.; Yaghi, O. M. *J. Am. Chem. Soc.* **2005**, *127*, 17998. (d) Furukawa, H.; Miller, M. A.; Yaghi, O. M. *J. Mater. Chem.* **2007**, *17*, 3197. (e) Ma, S.; Sun, D.; Simmons, J. M.; Collier, C. D.; Yuan, D.; Zhou, H. C. *J. Am. Chem. Soc.* **2008**, *130*, 1012. (f) Morris, R. E.; Wheatley, P. S. *Angew. Chem., Int. Ed.* **2008**, *47*, 4966. (g) Llewellyn, P. L.; Bourrelly, S.; Serre, C.; Vimont, A.; Daturi, M.; Hamon, L.; De Weireld, G.; Chang, J.-S.; Hong, D.-Y.; Hwang, Y. K.; Jhung, S. H.; Férey, G. *Langmuir* **2008**, *24*, 7245. (h) Furukawa, H.; Ko, N.; Go, Y. B.; Aratani, N.; Choi, S. B.; Choi, E.; Yazaydin, A. Ö.; Snurr, R. Q.; O’Keeffe, M.; Kim, J.; Yaghi, O. M. *Science* **2010**, *329*, 424.

(2) EERE: Hydrogen, Fuel Cells, & Infrastructure Technologies Program, <http://www.eere.energy.gov/hydrogenandfuelcells> (accessed August 2010).

(3) (a) Rosi, N. L.; Eckert, J.; Eddaoudi, M.; Vodak, D. T.; Kim, J.; O’Keeffe, M.; Yaghi, O. M. *Science* **2003**, *300*, 1127. (b) Férey, G.; Latroche, M.; Serre, C.; Millange, F.; Loiseau, T.; Percheron-Guégan, A. *Chem. Commun.* **2003**, 2976. (c) Rowsell, J. L.; Millward, A. R.; Park, K. S.; Yaghi, O. M. *J. Am. Chem. Soc.* **2004**, *126*, 5666. (d) Lee, E. Y.; Suh, M. P. *Angew. Chem., Int. Ed.* **2004**, *43*, 2798. (e) Sun, D.; Ma, S.; Ke, Y.; Collins, D. J.; Zhou, H.-C. *J. Am. Chem. Soc.* **2006**, *128*, 3896. (f) Wong-Foy, A. G.; Matzger, A. J.; Yaghi, O. M. *J. Am. Chem. Soc.* **2006**, *128*, 3494. (g) Lin, X.; Jia, J.; Zhao, X.; Thomas, K. M.; Blake, A. J.; Walker, G. S.; Champness, N. R.; Hubberstey, P.; Schröder, M. *Angew. Chem., Int. Ed.* **2006**, *45*, 7358. (h) Latroche, M.; Surlblé, S.; Serre, C.; Mellot-Draznieks, C.; Llewellyn, P. L.; Lee, J.-H.; Chang, J.-S.; Jhung, S. H.; Férey, G. *Angew. Chem., Int. Ed.* **2006**, *45*, 8227. (i) Xiao, B.; Wheatley, P. S.; Zhao, X.; Fletcher, A. J.; Fox, S.; Rossi, A. G.; Megson, I. L.; Bordiga, S.; Regli, L.; Thomas, K. M.; Morris, R. E. *J. Am. Chem. Soc.* **2007**, *129*, 1203. (j) Kaye, S. S.; Dailly, A.; Yaghi, O. M.; Long, J. R. *J. Am. Chem. Soc.* **2007**, *129*, 14176. (k) Sumida, K.; Hill, M. R.; Horike, S.; Dailly, A.; Long, J. R. *J. Am. Chem. Soc.* **2009**, *131*, 15120. (l) Murray, L. J.; Dincă, M.; Long, J. R. *Chem. Soc. Rev.* **2009**, *38*, 1294 and references therein.

(4) Bhatia, S. K.; Myers, A. L. *Langmuir* **2006**, *22*, 1688.

(5) (a) Garrone, E.; Bonelli, B.; Otero Areán, C. *Chem. Phys. Lett.* **2008**, *456*, 68. (b) Otero Areán, C.; Chavan, S.; Cabello, C. P.; Garrone, E.; Palomino, G. T. *ChemPhysChem* **2010**, *11*, 3237.

(6) (a) Dietzel, P. D. C.; Morita, Y.; Blom, R.; Fjellvag, H. *Angew. Chem., Int. Ed.* **2005**, *44*, 6354. (b) Dincă, M.; Long, J. R. *J. Am. Chem. Soc.* **2005**, *127*, 9376. (c) Rosi, N. L.; Kim, J.; Eddaoudi, M.; Chen, B.; O’Keeffe, M.; Yaghi, O. M. *J. Am. Chem. Soc.* **2005**, *127*, 1504. (d) Vimont, A.; Goupil, J.-M.; Lavalley, J.-C.; Daturi, M.; Surlblé, S.; Serre, C.; Millange, F.; Férey, G.; Audebrand, N. *J. Am. Chem. Soc.* **2006**, *128*, 3218. (e) Moon, H. R.; Kobayashi, N.; Suh, M. P. *Inorg. Chem.* **2006**, *45*, 8672. (f) Dincă, M.; Dailly, A.; Liu, Y.; Brown, C. M.; Neumann, D. A.; Long, J. R. *J. Am. Chem. Soc.* **2006**, *128*, 16876. (g) Dietzel, P. D. C.; Panella, B.; Hirscher, M.; Blom, R.; Fjellvag, H. *Chem. Commun.* **2006**, 959. (h) Dincă, M.; Han, W. S.; Liu, Y.; Dailly, A.; Brown, C. M.; Long, J. R. *Angew. Chem., Int. Ed.* **2007**, *46*, 1419. (i) Dincă, M.; Long, J. R. *Angew. Chem., Int. Ed.* **2008**, *47*, 6766. (j) Caskey, S. R.; Wong-Foy, A. G.; Matzger, A. J. *J. Am. Chem. Soc.* **2008**, *130*, 10870. (k) Dietzel, P. D. C.; Blom, R.; Fjellvag, H. *Eur. J. Inorg. Chem.* **2008**, 3624. (l) Liu, Y.; Kabbour, H.; Brown, C. M.; Neumann, D. A.; Ahn, C. C. *Langmuir* **2008**, *24*, 4772. (m) Dietzel, P. D. C.; Johnsen, R. E.; Fjellvag, H.; Bordiga, S.; Groppo, E.; Chavan, S.; Blom, R. *Chem. Commun.* **2008**, 5125. (n) Zhou, W.; Wu, H.; Yildirim, T. *J. Am. Chem. Soc.* **2008**, *130*, 15268. (o) Dietzel, P. D. C.; Besikiotis, V.; Blom, R. *J. Mater. Chem.* **2009**, *19*, 7362. (p) Sumida, K.; Horike, S.; Kaye, S. S.; Herm, Z. R.; Queen, W. L.; Brown, C. M.; Grandjean, F.; Long, G. J.; Dailly, A.; Long, J. R. *Chem. Sci.* **2010**, *1*, 184.

(7) Belof, J. L.; Stern, A. C.; Eddaoudi, M.; Space, B. *J. Am. Chem. Soc.* **2007**, *129*, 15202.

(8) Cheon, Y. E.; Suh, M. P. *Chem. Commun.* **2009**, 2296.

(9) Vitillo, J. G.; Regli, L.; Chavan, S.; Ricchiardi, G.; Spoto, G.; Dietzel, P. D. C.; Bordiga, S.; Zecchina, A. *J. Am. Chem. Soc.* **2008**, *130*, 8386.

(10) (a) Frost, H.; Düren, T.; Snurr, R. Q. *J. Phys. Chem. B* **2006**, *110*, 9565. (b) Han, S. S.; Deng, W.-Q.; Goddard, W. A. *Angew. Chem., Int. Ed.* **2007**, *46*, 6289. (c) Han, S. S.; Goddard, W. A. *J. Am. Chem. Soc.* **2007**, *129*, 8422. (d) Thornton, A. W.; Nairn, K. M.; Hill, J. M.; Hill, A. J.; Hill, M. R. *J. Am. Chem. Soc.* **2009**, *131*, 10662. (e) Han, S. S.; Furukawa, H.; Yaghi, O. M.; Goddard, W. A. *J. Am. Chem. Soc.* **2009**, *131*, 11580. (f) Düren, T.; Bae, Y.-S.; Snurr, R. Q. *Chem. Soc. Rev.* **2009**, *38*, 1237 and references therein.

(11) Murray, L. J.; Dincă, M.; Yano, J.; Chavan, S.; Bordiga, S.; Brown, C. M.; Long, J. R. *J. Am. Chem. Soc.* **2010**, *132*, 7856.

(12) (a) Chui, S. S.-Y.; Lo, S. M.-F.; Charmant, J. P. H.; Orpen, A. G.; Williams, I. D. *Science* **1999**, *283*, 1148. (b) Vishnyakov, A.; Ravikovitch, P. I.; Neimark, A. V.; Bülow, M.; Wang, Q. M. *Nano Lett.* **2003**, *3*, 713. (c) Bordiga, S.; Regli, L.; Bonino, F.; Groppo, E.; Lamberti, C.; Xiao, B.; Wheatley, P. S.; Morris, R. E.; Zecchina, A. *Phys. Chem. Chem. Phys.* **2007**, *9*, 2676.

(13) Despite the ubiquitous nature of molecular paddlewheel chemistry, reports of metal–organic frameworks exhibiting the $M_3(\text{BTC})_2$ ($M = \text{Cr}, \text{Cu}$) structure type have been relatively limited. $\text{Mo}_3(\text{BTC})_2$: Kramer, M.; Schwarz, U.; Kaskel, S. *J. Mater. Chem.* **2006**, *16*, 2245. $[\text{Fe}_2(\text{H}_2\text{O})_2(\text{BTC})_{4/3}]\text{Cl}\cdot 4.5(\text{DMF})$: Xie, L.; Liu, S.; Gao, C.; Cao, R.; Cao, J.; Sun, C.; Su, Z. *Inorg. Chem.* **2007**, *46*, 7782.

(14) Certain commercial suppliers are identified in this paper to foster understanding. Such identification does not imply recommendation or endorsement by the National Institute of Standards and Technology, nor does it imply that the materials or equipment identified are necessarily the best available for the purpose.

(15) Toby, B. H. *J. Appl. Crystallogr.* **2001**, *34*, 210.

(16) Larson, A. C.; Von Dreele, R. B. *General Structure Analysis System (GSAS)*, Los Alamos National Laboratory Report LAUR 86-748, 2000.

(17) Brown, C. M.; Liu, Y.; Yildirim, T.; Peterson, V. K.; Kepert, C. J. *Nanotechnology* **2009**, *20*, 204025.

(18) Udovic, T. J.; Brown, C. M.; Leao, J. B.; Brand, P. C.; Jiggetts, R. D.; Zeitoun, R.; Pierce, T. A.; Peral, I.; Copley, J. R. D.; Huang, Q.; Neumann, D. A.; Fields, R. J. *Nucl. Instrum. Methods Phys. Res., Sect. A* **2008**, *588*, 406.

(19) Azuah, R. T.; Kneller, L. R.; Qiu, Y.; Tregenna-Piggott, P. L. W.; Brown, C. M.; Copley, J. R. D.; Dimeo, R. M. *J. Res. Natl. Inst. Stand. Technol.* **2009**, *114*, 241.

(20) FitzGerald, S. A.; Churchill, H. O. H.; Korngut, P. M.; Simmons, C. B.; Strangas, Y. E. *Rev. Sci. Instrum.* **2006**, *77*, 093110.

(21) Rowsell, J. L. C.; Yaghi, O. M. *J. Am. Chem. Soc.* **2006**, *128*, 1304.

(22) Peterson, V. K.; Liu, Y.; Brown, C. M.; Kepert, C. J. *J. Am. Chem. Soc.* **2006**, *128*, 15578.

(23) The shortest $M^{2+}-D_2$ distance directly observed to date within a metal–organic framework via neutron diffraction is 2.15(4) Å observed within $\text{Fe}_3[(\text{Fe}_4\text{Cl})_3(\text{BTT})_8]_2$ ($\text{Fe}-\text{BTT}$, $\text{BTT}^{3-} = 1,3,5$ -benzenetrisulfonate), which features unsaturated Fe^{2+} coordination sites; see ref 6p.

(24) Ramirez-Cuesta, A. J.; Mitchell, P. C. H.; Ross, D. K.; Georgiev, P. A.; Anderson, P. A.; Langmi, H. W.; Book, D. *J. Mater. Chem.* **2007**, *17*, 2533.

(25) Note that the correlation between the neutron scattering data and infrared data is not definitive owing to the difference in the conditions (temperature and loading level) employed for the two types of experiments. While the analysis presented here allows the greatest degree of consistency and agreement between the two types of data, we envisage a number of alternative scenarios for peak assignment (particularly for site I and II), if the infrared data alone is considered.

NOTE ADDED AFTER ASAP PUBLICATION

This article was published ASAP on March 25, 2011. A text correction has been made in the last paragraph before the Conclusions and another in ref 23. The correct version was published on April 1, 2011.